Faraday
Discussions

Accepted Manuscript

Faraday Discussions

Royal Society of Chemistry

ROYAL SOCIETY OF CHEMISTRY

ROYAL SOCIETY
OF CHEMISTRY

www.rsc.org/faraday_d

Journal Name

ARTICLE

Evaluation of oxide ceramics as anodes for SOECs

A. Egger,[a] N. Schrödl[a] and W. Sitte[a]

$La_2NiO_{4+\delta}$ is characterised as an example for a potential anode material for high-temperature solid oxide electrolyser cells (SOECs). Short-term characterisation is performed from 700°C to 850°C between 0.01 and 1 bar oxygen partial pressure (pO_2) on asymmetrical cells using $Ce_{0.9}Gd_{0.1}O_{2-\delta}$ as electrolyte. Long-term degradation studies over more than 3000 hours are conducted at 800°C and 0.2 bar pO_2 in dry and humid atmospheres with and without a Cr-source placed in close vicinity to the cell. The SOEC anode performance is investigated by current-voltage curves combined with impedance spectroscopy. Current densities of up to -410 mAcm^{-2} are applied in current-voltage measurements and during long-term degradation studies. A total increase in anode resistance by 350% is observed over the course of the degradation measurements in increasingly harsh environment. Post-test analyses by SEM/EDX on a polished cross section of the cell show the presence of several contaminants in the electrode structure. However, chromium has not been identified by EDX even after prolonged exposure to Cr-sources in humid atmospheres, which is attributed to the anodic polarisation of the electrode. Electrode delamination appears to be the main factor for the strong loss in performance.

Introduction

Increasing production of electrical energy from renewables such as wind power or photovoltaics requires large-scale storage capacities to compensate for production fluctuations and to bridge the gap between energy supply and demand. Currently, intense research is devoted to high-temperature (HT) electrolysers, which operate at temperatures above 600°C. They feature high conversion efficiencies, especially when thermally coupled to existing infrastructure such as power plants or industrial facilities. HT-electrolysers can be used to generate hydrogen by water splitting as well as for the production of syngas when operated with H_2O/CO_2-mixtures. SOEC research and development can draw on the extensive body of knowledge acquired in the field of solid oxide fuel cells (SOFCs).

Similar to SOFC technology, long-term stability of SOE cells is a major issue. A prevalent degradation mode for SOECs is delamination of the anode (oxygen electrode) observed during steam electrolysis[1]. Another issue – of high importance in SOFC electrodes – is poisoning of the air electrode by impurities such as Cr released from metallic interconnects or balance-of-plant components[2]. The transport of chromium into the porous electrode proceeds through gas phase transport of volatile Cr species. Chromium in its highest oxidation state has relevant partial pressures with CrO_3 being the dominant gas species under dry and oxidising conditions. Moreover, Cr transport is strongly enhanced in the presence of water due to the higher volatility of the corresponding mono-hydrate H_2CrO_4 in humid atmospheres[3]. For SOFC cathodes the deposition of chromium at the surface or triple phase boundaries of the electrode has often been attributed to the cathodic polarisation mode[3-7], where electrochemical reduction or low oxygen partial

pressures under operating conditions appear to enhance deposition of Cr(III) species. It is thus interesting to see if Cr-poisoning poses less problems to SOEC oxygen electrodes under anodic polarisation.

In this work, $La_2NiO_{4+\delta}$ (LNO) is investigated with respect to its suitability and long-term stability as SOEC anode. The investigated compound is free of alkaline earth elements which is considered to be beneficial for long-term stability since many degradation modes in SOFCs are known to originate from - or to be aggravated by - the presence of alkaline earth metals[8-13]. Long-term durability is tested at 800°C for 140 days (~3300 hours) applying current densities up to -410 mAcm^{-2} under pure Ar/O_2 atmospheres as well as in the presence of chromium and humidity.

Experimental

Powders of $La_2NiO_{4+\delta}$ (LNO) and $Ce_{0.9}Gd_{0.1}O_{2-\delta}$ (CGO) were obtained from Treibacher Industrie AG. Screen printing pastes of LNO were produced externally (Fraunhofer IKTS, Germany) as well as in-house by dispersing the powder in a commercial ink vehicle and using a three roll mill (Exakt 50I) for homogenisation.

Dense electrolyte substrates were obtained by uniaxially pressing CGO powder in a stainless steel die (2 cm Ø) at 1 ton and sintering for 10 hours at 1450°C in air. Typical dimensions of the sintered electrolyte pellets were 16 mm diameter and 1.6 mm thickness with a relative density of above 95%. A thin groove was cut along the circumference of the CGO tablets and a Pt-wire was fixed with Pt-paste into the notch serving as reference electrode. On one side of the CGO substrates a Pt-

grid was attached with Pt-paste as counter electrode. On the other side of the substrates an LNO layer was applied via screen printing and sintered for 2 h between 1200°C and 1250°C in air. The thickness of the LNO electrodes ranged between 17 and 30 μm as determined by SEM from cell cross sections. The LNO layers were contacted by means of a gold grid attached with gold paste, since gold is known to be catalytically inactive for the oxygen redox reaction.

Each cell was mounted in an alumina tube located inside a horizontal tubular furnace. Short-term measurements were conducted between 700 and 850°C in an atmosphere of 20% O_2 in argon at a flow rate of 2 L/h. Electrochemical characterisation was performed by means of current-voltage curves and impedance analysis in open circuit conditions (OCV) and under load. Current bias was applied such that oxygen was pumped through the CGO electrolyte from the Pt-side to the LNO side, thus operating the LNO electrode as an SOEC anode under current bias. For impedance analysis the frequency response analyser (Alpha-A with POT/GAL interface, Novocontrol) was set to three-electrode, 4-wire galvanostatic mode with perturbation amplitudes between 1 and 10 mA (r.m.s.) and a frequency range of 100 mHz to 1 MHz.

Long-term investigations of Cr-degradation at the anode side were performed at 800°C in dry and humid atmospheres. Cr-poisoning was achieved by placing small chromium chips (99.996% purity) in the reactor upstream of the sample cell. Humidification of the gas stream was accomplished by passing the gas stream through a water bubbler thermostatted at 6°C which corresponds to an equilibrium partial pressure of water of 9.4 mbar or 30% relative humidity (r.h.) at 25°C.

Cell cross sections were obtained by cutting the sample with a diamond wire saw, embedding in cold-curing resin, grinding and polishing with diamond suspensions with a final particle size of 1 μm. Post-test microstructural analysis was performed using a scanning electron microscope (SEM) Zeiss EVO 50, Germany, with LaB_6-cathode and EDX-detector (Oxford Instruments).

Methodology

A schematic of the cell design employed in this work is shown in Fig. 1. In an early stage of the degradation study the cell design was changed from symmetric to asymmetric due to delamination issues of the LNO counter electrode after applying large bias currents. Since a reference electrode was used for all electrochemical measurements, the cell´s counter electrode was replaced by a porous Pt-layer expecting to have little effect on results obtained for the SOEC anode side.

CGO was used as electrolyte material due to its high ionic conductivity and low reactivity with LNO at higher temperatures[14]. Electrolytes of real SOEC cells are not expected to be made of ceria due to electronic contributions to the total conductivity under reducing conditions, resulting in internal short-circuiting of the cell. However, a protective barrier layer of CGO at the oxygen electrode side is very common and thus the SOEC anode side is well represented by the cell design used in this work.

All electrochemical measurements were conducted against a Pt-reference electrode mounted at the circumference of the electrolyte substrate. The equivalent circuit used to model the impedance response is shown in Fig. 2, where L_0 is the inductance of the setup, R_0 the bulk resistance of the electrolyte,

R_1 the grain boundary resistance of the electrolyte, and R_2, R_3 resistances of processes occurring at the SOEC anode.

The validation of the above assignment was based mainly on the order-of-magnitude values obtained for capacitances C. The capacitances were calculated from the fitting values of the constant phase elements (CPEs) used to model the capacitive contributions of the processes (Fig. 2) according to Eq. (1) [15]

$$C_i = R_i^{\frac{1}{n_i}-1} Q_i^{\frac{1}{n_i}} \qquad (1)$$

where n_i and Q_i are parameters defining the CPE admittance[16] via $Y_{CPE} = Q(jw)^n$. Values of C of grain boundaries could be obtained from measurements below 800°C and were in the range of several tens of nF, while capacitances of processes in the low-frequency part of the spectra were above 100 μF and thus attributed to anode processes. No attempts were made for a more detailed assignment of anode processes to impedance elements in the equivalent circuit. The main point of the impedance measurements was to separate the lead inductance and electrolyte contributions from the SOEC electrode part.
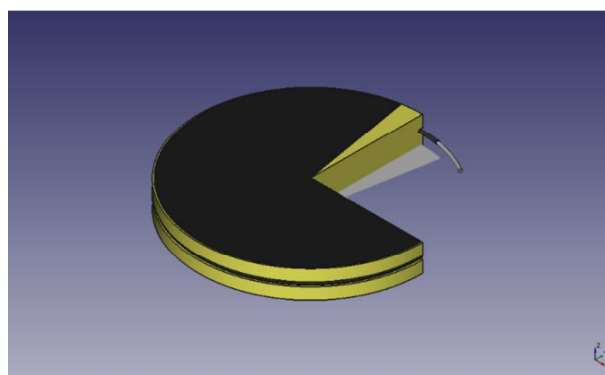
Fig. 1. Schematic of the asymmetric cell design used to evaluate SOEC anode performance. Layer structures from bottom to top are: Pt-counter electrode, CGO electrolyte with Pt-reference along the circumference, LNO anode as working electrode.

Anode performance was investigated by means of current-voltage (I/U) curves up to current densities of -410 $mAcm^{-2}$. I/U-measurements were complemented by impedance analysis under load over the same current range to correct for the electrolyte contribution.
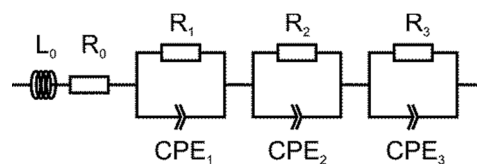
Fig. 2. Equivalent circuit used to model impedance spectra with inductance L_0, resistances R_i and constant phase elements CPE_i.

Fig. 3 shows examples of impedance spectra under increasing current bias. Blue lines correspond to fitting curves based on

the equivalent circuit given in Fig. 2. Shifts of the high frequency intercepts on the real axis are caused by Joule heating of the sample during current load. The temperature increase of the sample at different current bias was measured separately with a thermocouple pressed onto the anode layer. A maximum temperature change of +15°C was observed at 800°C for current densities of around -450 mAcm^{-2}, which is consistent with the observed decrease in the electrolyte contribution in Fig. 3.
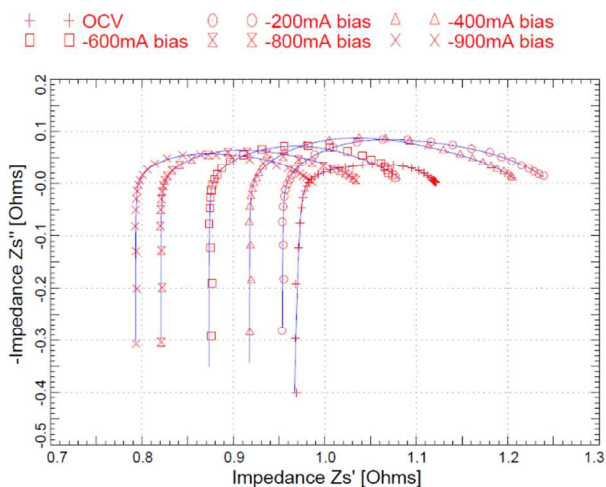
Fig. 3. Impedance spectra of an LNO electrode as SOEC anode at 800°C under current load. Data points are plotted in red colour, blue lines are fitting curves obtained from non-linear complex regression analysis.

Results and discussion

Short-term characterisation

SEM-images of sintered anode layers (Fig. 4) confirm good connectivity of the LNO grains while retaining sufficient porosity for gas diffusion of oxygen through the electrode to the surroundings.
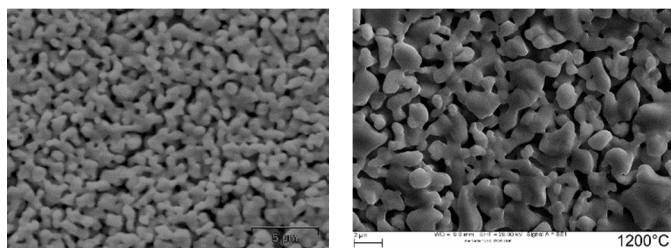
Fig. 4. Top view of screen printed LNO anode layers used for short-term characterisation (left) and Cr-poisoning studies (right) sintered at 1200°C and 1250°C, respectively, for 2 h in air.

Impedance spectra under OCV conditions at 0.2 bar pO_2 are shown in Fig. 5 where contributions from the electrolyte and measurement setup have been subtracted. ASR values of the LNO electrode are 2.16, 0.78, 0.30 and 0.19 Ωcm^2 at 700, 750, 800 and 850°C, respectively. Impedance data indicate at least two sub-processes on the anode side with an overall activation energy of 240 kJmol^{-1}. C-values of the low and high-frequency

arcs are around 1×10^{-2} and 5×10^{-4} Fcm^{-2}, respectively, and do not change significantly within the temperature range investigated.
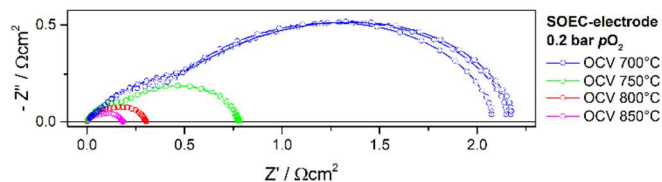
Fig. 5. OCV impedance spectra of an LNO electrode between 700 and 850°C in 20% O$_2$/Ar. Lines are guides to the eye.

Reducing the oxygen partial pressure has a significant influence on anode polarisation, as shown in Fig. 6. While increasing the pO_2 to 1 bar causes only a slight reduction in electrode polarisation, changing the gas phase to 1% O$_2$/Ar increases the ASR to almost 1 Ωcm^2 at 800°C. In addition, a third electrode process emerges at low pO_2 as indicated by the appearance of a third semicircle in the impedance spectra. The latter point can be appreciated more clearly in Fig. 7, where the imaginary part Z'' is plotted as a function of frequency.
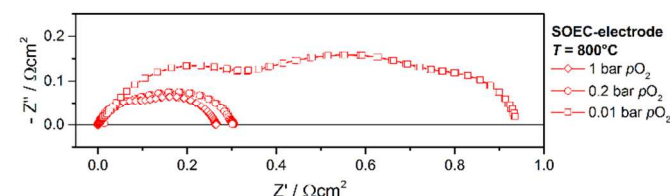
Fig. 6. OCV impedance spectra of an LNO-electrode at 800°C and oxygen partial pressures between 0.01 and 1 bar. Lines are guides to the eye.

Peak frequencies of the sub-processes can be estimated from Fig. 7. Electrolyte and setup contributions have been removed in Figs. 6 and 7. For fitting the impedance data at 0.01 bar pO_2 an additional R||CPE-element has been incorporated in the equivalent circuit shown in Fig. 2.
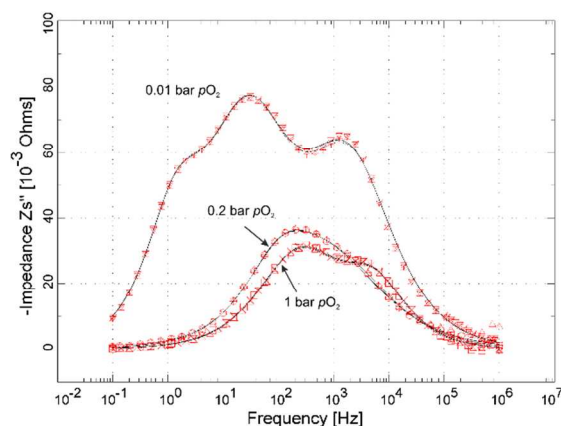
Fig. 7. Reactance of impedance data plotted in Fig. 6 vs. frequency at 800°C and different pO_2. Red symbols are data points, fitting curves are shown as black lines.

Long-term investigation

The long-term stability of LNO as SOEC anode was investigated at 800°C over a period of 140 days (3300 h) under continuous current load of -410 mAcm^{-2}. After 46 days (1100 h) in pure 20% O$_2$/Ar atmosphere Cr was added under dry conditions and after another 41 days (1000 h) 30% relative humidity was introduced into the gas stream. Figs. 8 and 9 show OCV impedance data and I/U-curves in dry and humid atmospheres with a Cr-source placed close to the sample. Electrolyte contributions are separated and subtracted from I/U-data by means of impedance measurements. Current-voltage curves show significant non-linearity at higher current densities which is probably caused by Joule heating of the cell.

The results in Fig. 8 show that electrode deterioration proceeds rather slowly in the first 30 days after Cr-insertion but accelerates in the subsequent 10 days. The total increase in anode ASR is around 50% in this period.
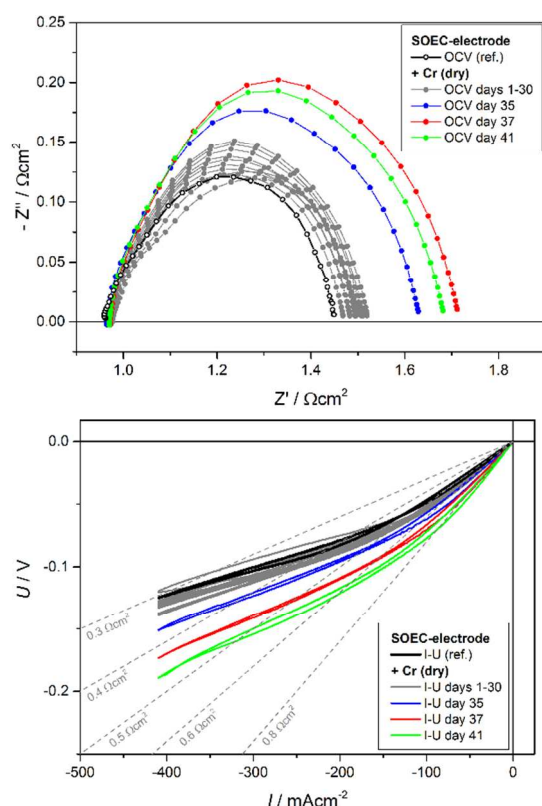
Fig. 8. OCV impedance spectra (top) and I/U-curves (bottom) of an LNO anode at 800°C in dry 20% O$_2$/Ar in the presence of a Cr-source. Electrolyte resistance has been subtracted in I/U-curves. Results from the last measurement before introducing the Cr-source are shown for comparison ("ref.").

A similar trend is observed after humidification of the gas stream (Fig. 9). Degradation rates are comparatively low at the beginning but increase after prolonged exposure to 30% relative humidity. Based on OCV impedance data the increase in anode ASR after 41 days in Cr/H$_2$O-containing atmospheres amounts to ~35%.
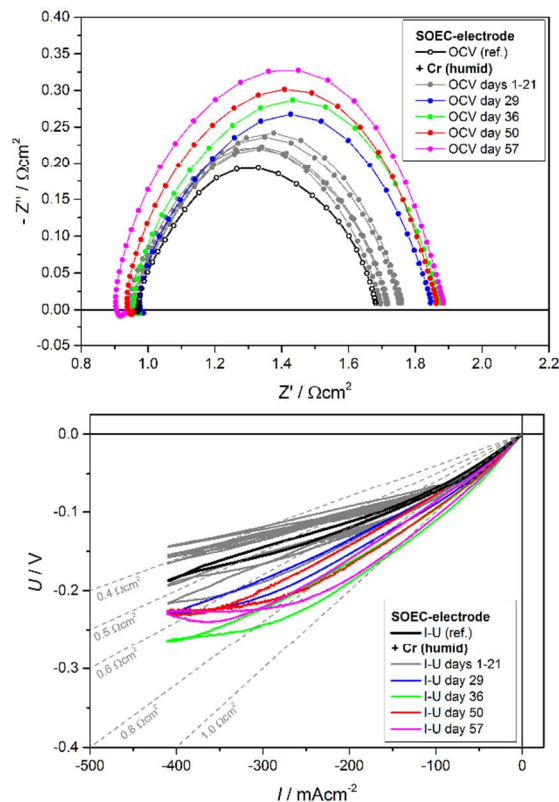
Fig. 9. OCV impedance spectra (top) and I/U-curves (bottom) of an LNO anode exposed to a Cr-source in 20% O$_2$/Ar with 30% relative humidity at 800°C. Electrolyte contributions have been removed from I/U-curves. Results from the last measurement before starting gas humidification are given for comparison ("ref.").

ASR values of the SOEC anode (R_{pol}) and the CGO electrolyte (R_s) were determined from OCV impedance spectra over the whole degradation period (Fig. 10). R_{pol} of the fresh LNO anode is around 0.2 Ωcm^2 and was found to decrease in the first 10 days, after which a continuous increase in polarisation resistance is observed. After three weeks, distortions appearing in the impedance spectra indicated cell failure and the cell was cooled to room temperature and visually inspected. Complete delamination of the LNO counter electrode was found and cell tests were continued after applying Pt-paste/Pt-grid as new counter electrode. The reason for the delamination of the SOFC electrode is unclear but has been reproduced in a separate experiment with another symmetrical LNO cell under current load. Reducing conditions on the cathode side might have caused slow decomposition of the LNO counter electrode. However, based on results from Nakamura et al.[17], such decomposition would require effective oxygen partial pressures of below 10^{-15} bar at 800°C. A discontinuity in R_{pol} and - less pronounced - in R_s is observed after replacement of the counter electrode (Fig. 10), which suggests that data before the delamination issue are of limited accuracy and may have been shifted to too low ASR values. Furthermore, the sintering step necessary to attach the freshly applied Pt-counter electrode to the electrolyte might also have affected the microstructure of the porous SOEC anode.

General trends regarding the effect of Cr and humidity on anode deterioration are difficult to establish based on impedance and I/U-data obtained in this work. Degradation

rates for R_{pol} are similar between all three time segments shown in Fig. 10 and are thus likely to be caused by the current load rather than by poisoning processes. A strong increase in anode ASR toward the end of the second stage (i.e. Cr in dry atmospheres) might indicate a Cr-poisoning effect setting in after some induction period. Shortly after humidification of the gas stream the anode ASR was found to recover, but after several days degradation resumed at rates similar to the previous ones. During the whole degradation study R_{pol} increased by 350% from 0.22 to 1.0 Ωcm^2, whereas the electrolyte contribution R_s remained practically constant. More insight regarding the contribution of chromium and humidity to the anode degradation was obtained from analytical examination of cross sections of the tested cell.
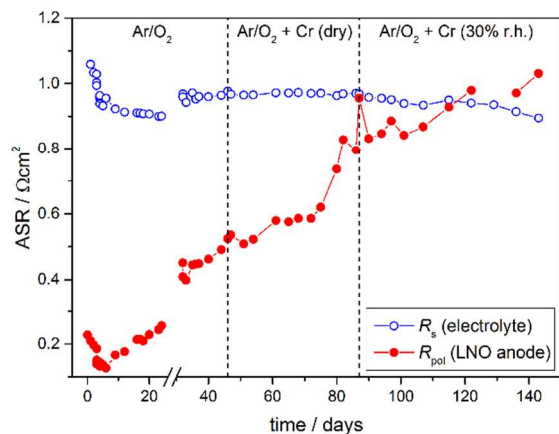
Fig. 10. Trends in electrolyte resistance (R_s) and polarisation resistance (R_{pol}) of an LNO anode under constant current load of -410 mAcm^{-2}. The discontinuity in ASR at day 24 marks the replacement of the LNO counter electrode by a porous Pt-layer.

Post-test analysis

Visual inspection of the cell after the measurements showed no signs of delamination of the anode layer from the electrolyte. An SEM picture of a polished cross section of the cell after finishing long-term investigations are given in Fig. 11. The image shows the screen printed anode layer of uniform thickness (29 μm) deposited on the CGO electrolyte containing some residual porosity. Foreign phases can be discerned in the anode layer by material contrast.

Several impurity phases have been identified by EDX analysis in the upper half of the anode layer (Fig. 12). Bright patches are due to gold, probably caused by the polishing procedure since the Au-current collector has been cut and polished together with the sample. In the upper half of the anode layer light-grey textures are visible in the surface region of the LNO particles containing significant amounts of bismuth. Bi is used as additive in the gold paste to improve sinterability but is found to diffuse into the porous electrode structure and further into the LNO bulk. From the rather finely dispersed distribution of the Bi-containing phase it appears that diffusion proceeds mainly along grain boundaries.

Peaks of Ir and Rh have also been identified in the EDX spectra. Ir may originate from Pt-components containing iridium impurities while rhodium is introduced via an S-type thermocouple with Pt/Rh-protection sheath placed close to the sample. Moreover, the surface of the SOEC anode layer is covered by a Si-containing scale (Fig. 12), whose origin is unclear. The silicon content of the LNO raw powder is quite low (~90 ppm) and the measurement setup does not contain any apparent silicon sources.

The above-mentioned impurities are considered to be insignificant with respect to electrode performance. Ir and Rh are found only sporadically as isolated inclusions within the SOEC anode. The presence of Si is restricted to the gas/anode interface which seems to be less critical with respect to the drastic loss in anode performance. Bi-contaminations are spread throughout the porous electrode structure but appear to be accumulated in the outer part of the anode layer and less concentrated in the electroactive region close to the electrolyte. Moreover, superficial Bi-contamination of the related nickelate compound $Nd_2NiO_{4+\delta}$ has been shown previously to be uncritical with respect to electrical conductivity and oxygen surface exchange activity[18].

Surprisingly, chromium could not been identified by EDXS even after long time exposure to Cr/H$_2$O-containing atmospheres. Detection of low concentrations of Cr next to a La/O-rich bulk phase by EDXS is difficult due to strong overlap of the Cr X-ray K_α and L_α emission lines with those of La and O[19]. However, larger amounts of Cr can be detected by a shift in the La L_α/L_β peak intensity ratios[20, 21].

EDX point spectra of the degraded anode yield intensity ratios of La-L signals which appear to be as expected for Cr-free material and thus chromium impurities – if present – may occur only in low concentrations in the anode structure. This finding is rather unexpected, since long-term investigations on dense LNO samples at 700°C[22] and 800°C[23] in Cr-containing atmospheres have shown significant impact on oxygen surface exchange kinetics and the deposition of Cr-species on the material surface has been clearly established[22].

The observed absence of chromium might be a consequence of the anodic polarisation of the SOEC electrode. This mode of operation could prevent degradation processes observed in Cr-poisoning of SOFC cathodes, where the conversion of gaseous Cr(VI)-species[24] to less volatile Cr(III)-compounds (e.g. Cr_2O_3) has been ascribed to electrochemical reduction[3-5] or low effective pO_2 at the electrode-electrolyte interface under cathodic current load[6, 7].
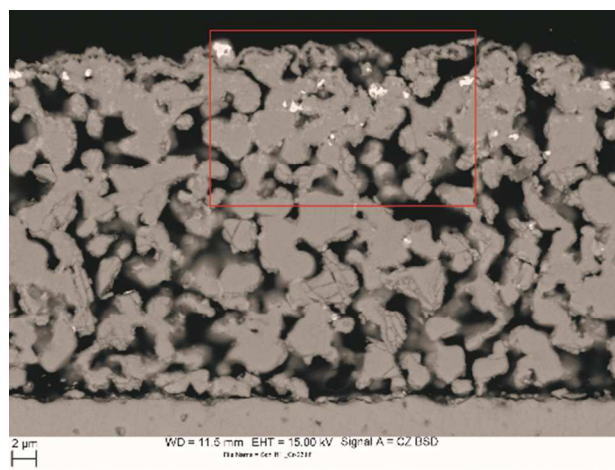
Fig. 11. Backscatter SEM image of a cross section of the LNO anode after long-term measurements. The picture shows a close-up view of the SOEC anode layer on top of the CGO electrolyte, the red outline marks a region analysed by EDX (see Fig. 12).

Cracks in the electrolyte, either intragranular or along grain boundaries, do not occur near the electrolyte-anode-interface, as has been reported in the literature for SOEC operation at high current densities[25, 26]. This is consistent with the fairly constant electrolyte resistance obtained from impedance measurements (see Fig. 10 and EIS spectra in Figs. 8 and 9).

EIS results clearly indicate the anode contribution being the main factor in the increasing performance loss. Close inspection of the anode micrographs in Figs. 11 and 12 shows several LNO grains in the SOEC layer to have been fractured but the main part of the porous anode framework appears to be undamaged. The electrode-electrolyte contact, however, appears to be rather poor which is a well-known degradation mode caused by long-term SOEC operation. Although mechanical delamination has not been observed upon removing the cell after testing, loss of electrode-electrolyte contact area may well account for the ongoing degradation under anodic load. This degradation mode may be even more dominant in the current type of single cell testing since the cell was not kept under compressive load during operation. It is thus concluded that an increase in the anode-electrolyte contact resistance due to a decreasing number of contact points is the main factor for the observed cell degradation.
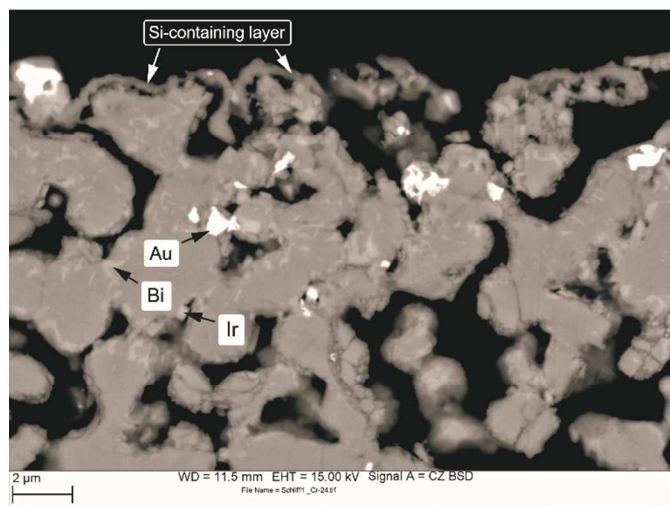
Fig. 12. SEM-EDX analysis of foreign phases identified in the SOEC anode layer after testing.

Conclusions

La$_2$NiO$_{4+\delta}$ was characterised as SOEC anode material on a Ce$_{0.9}$Gd$_{0.1}$O$_{2-\delta}$ electrolyte between 700 and 850°C and 0.2 bar oxygen partial pressure. ASR-values of the oxygen electrode at 800°C were determined as 0.22 and 0.30 Ωcm^2 for two different cells. Long-term investigations under constant current load of -410 mAcm^{-2} were performed over a period of 140 days at 800°C under dry conditions as well as in Cr/H$_2$O-containing atmospheres. A total increase in anode ASR by 350% from 0.22 to 1.0 Ωcm^2 was observed. A clear effect of Cr in dry/humid conditions on the degradation behaviour could not be determined from cell measurements. Post-test analysis on a cell cross section by EDXS revealed the presence of several impurities in the anode layer which are considered to be unlikely the reason for the marked degradation phenomena. Cr

has not been detected in the SOEC anode after long-term operation which indicates that Cr-poisoning may be less severe for LNO electrodes under anodic polarisation. Poor electrode/electrolyte contact or partial delamination – if caused during cell operation and not being a result of post-test sample preparation – is probably the largest contribution to the observed performance degradation of the LNO anode.

Notes and references

[a] Montanuniversitaet Leoben, Chair of Physical Chemistry, Franz-Josef-Strasse 18, 8700 Leoben, Austria.

1. M. A. Laguna-Bercero, *J. Power Sources*, 2012, **203**, 4-16.
2. J. R. Mawdsley, J. D. Carter, A. J. Kropf, B. Yildiz and V. A. Maroni, *Int. J. Hydrogen Energy*, 2009, **34**, 4198-4207.
3. K. Hilpert, D. Das, M. Miller, D. H. Peck and R. R. Weiss, *J. Electrochem. Soc.*, 1996, **143**, 3642-3647.
4. Y. Matsuzaki and I. Yasuda, *J. Electrochem. Soc.*, 2001, **148**, A126-A131.
5. S. P. S. Badwal, R. Deller, K. Foger, Y. Ramprakash and J. P. Zhang, *Solid State Ionics*, 1997, **99**, 297-310.
6. S. Taniguchi, M. Kadowaki, H. Kawamura, T. Yasuo, Y. Akiyama, Y. Miyake and T. Saitoh, *J. Power Sources*, 1995, **55**, 73-79.
7. M. Krumpelt, T. A. Cruse, B. J. Ingram, J. L. Routbort, S. Wang, P. A. Salvador and G. Chen, *J. Electrochem. Soc.*, 2010, **157**, B228-B233.
8. E. Bucher, A. Egger, G. B. Caraman and W. Sitte, *J. Electrochem. Soc.*, 2008, **155**, B1218-B1224.
9. E. Bucher, W. Sitte, F. Klauser and E. Bertel, *Solid State Ionics*, 2012, **208**, 43-51.
10. Y. Xiong, K. Yamaji, H. Teruhisa, H. Yokokawa, J. Akikusa, H. Eto and T. Inagaki, *J. Electrochem. Soc.*, 2009, **156**, B588-B592.
11. Z. Wuillemin, A. Nakajo, A. Müller, A. J. Schuler, S. Diethelm, J. Van Herle and D. Favrat, in *11th Intern. Symp. Solid Oxide Fuel Cells (SOFC-XI)*, ed. S. C. Singhal, The Electrochemical Society, Vienna, Austria, 2009, vol. 25 (2), pp. 457-466.
12. M. Kubicek, A. Limbeck, T. Frömling, H. Hutter and J. Fleig, *J. Electrochem. Soc.*, 2011, **158**, B727-B734.
13. E. Bucher, C. Gspan, F. Hofer and W. Sitte, *Solid State Ionics*, 2013, **230**, 7-11.
14. A. Montenegro-Hernández, J. Vega-Castillo, L. Mogni and A. Caneiro, *Int. J. Hydrogen Energy*, 2011, **36**, 15704-15714.
15. J. Fleig, *Solid State Ionics*, 2002, **150**, 181-193.
16. B. A. Boukamp, *Solid State Ionics*, 1986, **20**, 31-44.
17. T. Nakamura, K. Yashiro, K. Sato and J. Mizusaki, *Solid State Ionics*, 2009, **180**, 368-376.
18. A. Egger, W. Sitte, F. Klauser and E. Bertel, *J. Electrochem. Soc.*, 2010, **157**, B1537-B1541.
19. J. Andreas Schuler, P. Tanasini, A. Hessler-Wyser and J. V. herle, *Scripta Materialia*, 2010, **63**, 895-898.
20. M. C. Tucker, H. Kurokawa, C. P. Jacobson, L. C. De Jonghe and S. J. Visco, *J. Power Sources*, 2006, **160**, 130-138.

21. X. Chen, L. Zhang and S. P. Jiang, *J. Electrochem. Soc.*, 2008, **155**, B1093-B1101.
22. N. Schrödl, E. Bucher, A. Egger, P. Kreiml, C. Teichert, T. Höschen and W. Sitte, *Solid State Ionics*, 2015, accepted.
23. N. Schrödl, E. Bucher and A. Egger, in preparation.
24. B. B. Ebbinghaus, *Combust. Flame*, 1993, **93**, 119-137.
25. F. Tietz, D. Sebold, A. Brisse and J. Schefold, *J. Power Sources*, 2013, **223**, 129-135.
26. R. Knibbe, M. L. Traulsen, A. Hauch, S. D. Ebbesen and M. Mogensen, *J. Electrochem. Soc.*, 2010, **157**, B1209-B1217.

Faraday Discussions Accepted Manuscript